

Secondary Organic Aerosol Formation from Evaporated Biofuels: Comparison to Gasoline and Correcting for Vapor Wall Losses

Yicong He¹, Brandon King¹, Matson Pothier², Liam Lewane¹, Ali Akherati¹, James Mattila²,
Delphine K. Farmer², Robert McCormick³, Matthew Thornton³, Jeffrey R. Pierce⁴, John
Volckens¹, and Shantanu H. Jathar^{1*}

¹Department of Mechanical Engineering, Colorado State University, Fort Collins, CO, USA

²Department of Chemistry, Colorado State University, Fort Collins, CO, USA

³National Renewable Energy Laboratory, Golden, CO, USA

⁴Department of Atmospheric Science, Colorado State University, Fort Collins, CO, USA

*Correspondence to: Shantanu H. Jathar (shantanu.jathar@colostate.edu)

S1 HONO Synthesis

Measurements performed with a time-of-flight chemical ionization mass spectrometer (ToFwerk AG, Switzerland and Aerodyne Research Inc., MA) with an iodide reagent ion (Iodide-ToF-CIMS)¹⁻³ showed that the ‘wet’ HONO synthesis process of Ng et al.⁴ produced significantly higher concentrations of NO relative to HONO (NO:HONO~0.33 ppbv:a.u.) in the first 30 minutes, with much lower NO concentrations later (NO:HONO~0.06 ppbv:a.u.) (Figure S.2(a)). As the HONO concentrations peaked later than those for NO and were relatively flat between 40 and 60 minutes, venting the bubbler output for the first ~30 minutes and injecting for the next ~30 minutes meant that the initial NO (and also NO₂^{*}) concentrations during the chamber experiment were substantially lower with very little effect on the HONO concentrations. In our experiments, our NO and NO₂^{*} before lights were turned on was 46±15 and 160±60 ppbv, respectively, significantly lower than those in historical experiments that have used this synthesis process.^{4,5} Dropwise addition of NaNO₂ into a H₂SO₄ solution can also lead to reduced NO and NO₂ production but perhaps not to the same degree to the technique used in this work.⁴ We also experimented with bubbling clean air at ~1.3 L min⁻¹ through 80 mL of 10% H₂SO₄ and directing the H₂SO₄ vapors over solid NaNO₂ crystals before injecting the stream into the chamber. This synthesis process yielded a nearly 10-fold decrease in HONO emissions but with little to no NO production (Figure S.2(b)). This ‘dry’ synthesis process might allow for HONO to be used as an OH precursor without coproduction of NO and NO₂^{*}, but will need to be explored in future work. Experiments performed with HCl as a substitute to H₂SO₄ resulted in relatively little to no HONO production.

S2 SAPRC Modeling

We were unable to measure VOC concentrations and its decay during the fuel experiments and this prevented us from quantifying the OH concentrations during those experiments. Instead, we relied on OH concentrations predicted by the SAPRC99 gas-phase chemical mechanism. The ability of the model to predict OH was first demonstrated with dedicated chamber measurements performed with toluene, before being used to determine OH for the fuel experiments.

We performed four chamber experiments with toluene, identical to the methods used in the fuel experiments. However, in these experiments, we used a gas chromatograph photoionization detector (GC-PID; SRI Instruments, CA) to measure the decay of toluene and estimate OH concentrations and exposures. As shown in Figure S.3, the average OH exposure at the end of the experiment over those four toluene experiments was $(1.9 \pm 0.2) \times 10^7$ molecules-h cm⁻³. SAPRC99 was run using an offline version of the BOXMOX platform developed by Knote et al.

(2018). Chamber simulations were performed by specifying initial concentrations of NO, O₃, toluene (as ARO1), and HONO, photolysis rates for all species in SAPRC99, and the chamber temperature and relative humidity. Since the HONO synthesis method typically produces equal amounts of NO and NO₂ concentrations,⁶ we assumed the initial NO₂ to be equal to NO, although this assumption was not found to affect the findings from the SAPRC modeling. The photolysis rates for the chamber simulation were determined by scaling photolysis rates representative of UV-A lights (shared by Xuan Zhang, NCAR) to match the photolysis rate of NO₂ estimated from chemical actinometry experiments (0.25 min⁻¹; see Figure S.1). Since we did not measure HONO concentrations, we adjusted the initial HONO concentration till the model predictions agreed with the observations of O₃ and NO. We did not attempt to match the model predictions of NO₂ because the measurements were likely to include reactive nitrogen species other than NO₂ that were produced during the chamber experiment (e.g., nitric acid, peroxyacetyl nitrates). In Figure S.4, we show the model-measurement comparison for the OH exposure and the O₃ and NO concentrations for four toluene experiments. We found that our approach to model the gas-phase chemistry by constraining the model predictions to O₃ and NO seemed to reproduce the observed OH exposure in the toluene experiments.

Based on our success with modeling the toluene experiments, we used the same approach to model the gas-phase chemistry in the fuel experiments. The SAPRC simulations required us to map the VOC species in the fuels to appropriate surrogates in SAPRC99. This was done using published assignments suggested by William Carter (SpecDB.xls found at <https://intra.engr.ucr.edu/~carter/emitdb/>). While the assignments were relatively trivial for the alkanes, aromatics, and alkenes found in gasoline and ETH, SAPRC99 does not have appropriate surrogates to model the gas-phase chemistry of cyclopentanone, diisobutylene, 2-methylfuran, and dimethylfuran. Based on SpecDB.xls, cyclopentanone was modeled as MEK (methyl ethyl ketone), diisobutylene was modeled as OLE2 (alkenes with $k_{OH} > 4.77 \times 10^{-11} \text{ cm}^3 \text{ molecule}^{-1} \text{ s}^{-1}$), and furans were modeled as ARO2 (aromatics with $k_{OH} > 1.36 \times 10^{-11} \text{ cm}^3 \text{ molecule}^{-1} \text{ s}^{-1}$). Results for O₃ and NO from simulations performed on a representative ETH experiment are shown in Figure S.5(a) and predictions of OH exposure for all the fuel experiments are shown in Figure S.5(b). The OH exposure seemed to vary with the fuel, the amount of fuel injected, and the reactivity of the fuel. Generally, the OH exposure for the relatively less reactive fuels, cyclopentanone, gasoline, and ETH, was within the bounds of the OH exposures measured with the toluene experiments but the OH exposure was substantially lower for the more reactive fuels, diisobutylene (factor of ~2) and the alkylfuran mixture (factor of ~5).

In the future, we recommend the use of a proton transfer reaction - time of flight - mass spectrometer (PTR-ToF-MS) or a chemical ionization mass spectrometer (CIMS) to measure similar VOCs and their decay in the chamber experiments.⁷ Alternatively, or in addition, we suggest that simulations be performed with an explicit gas-phase chemical mechanism, the likes of MCM^{8,9} or GECKO-A¹⁰, to validate the OH data.

S3 Coefficient of Eddy Diffusion

We used the Aerosol Parameter Estimation (APE) model of Pierce et al.¹² with the scanning mobility particle sizer (SMPS, GRIMM Aerosol Technik, Austria) data to determine the coagulation-corrected, size-resolved wall loss rate ($k_{par,j}$, where j is the size bin) for particles up to 100 nm during the dark portions of the experiment when no SOA was being formed. The

calculations were only performed on data from six chamber experiments where we had access to sufficient SMPS data before the lights were turned on (minimum of 10 SMPS scans that showed uniform loss in particle number concentrations). We limited the calculations to particle sizes up to 100 nm because loss rates for larger sizes up to 1000 nm are strongly affected by the charge distribution on the particles and the Teflon® walls.^{13,14} These dark portions, over the six experiments, varied between 50 and 130 minutes. The $k_{par,j}$ values were then compiled together for all experiments to fit a study-wide $k_{w,p0}$ and k_e according to the following equation¹⁵:

$$k_{par,j} = \frac{1}{L} \left[\frac{8\sqrt{k_e D_j}}{\pi} + v_{s,j} \cdot \coth\left(\frac{x}{2}\right) \right] \text{ where } x = \frac{\pi v_{s,j}}{2\sqrt{k_e D_j}} \quad (5)$$

where D_j is the diffusion coefficient of the particle of size j in $m^2 s^{-1}$, L is one of the sides of the chamber assuming a cubical chamber in m (2.15 m) and $v_{s,j}$ is the gravitational settling velocity of the particle of size j in $m s^{-1}$.¹⁶ The $k_{par,j}$ for all the experiments performed in this work and the ensemble fit are shown in Figure S.6.

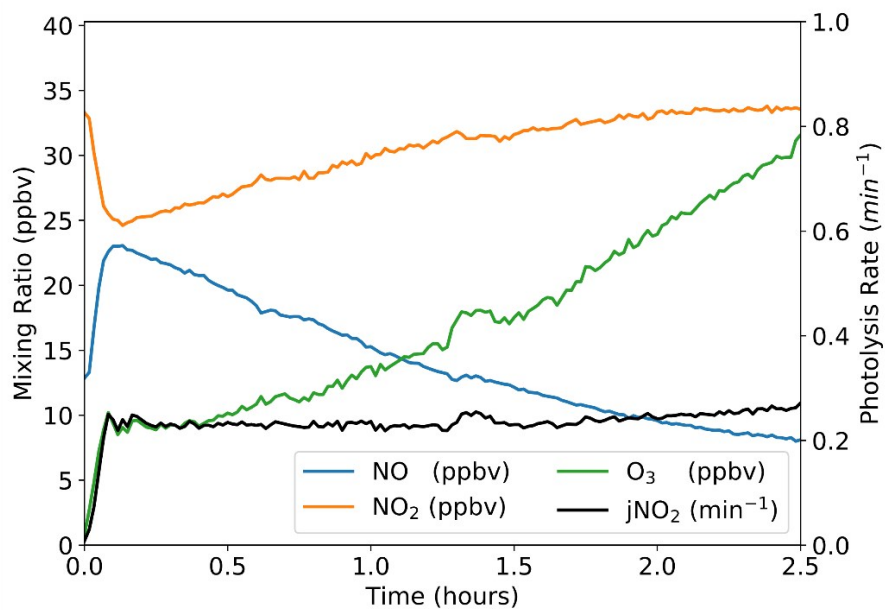


Figure S1: NO, NO₂ and O₃ concentrations and the NO₂ photolysis rate during the chemical actinometry experiment performed on May 20, 2016.

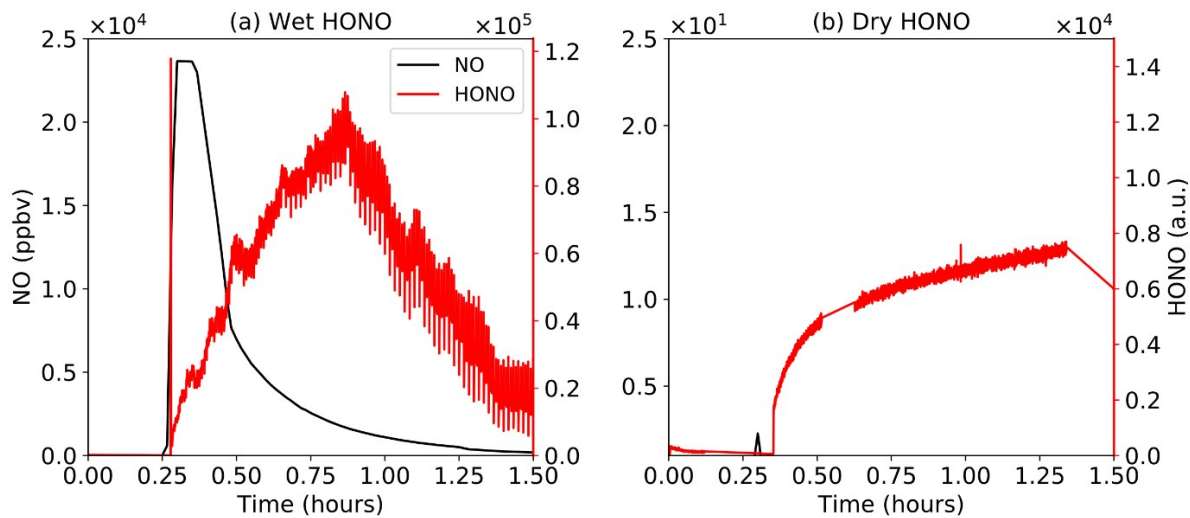


Figure S2: NO (ppbv) and HONO (arbitrary units) concentrations during the (a) wet and (b) dry HONO synthesis processes.

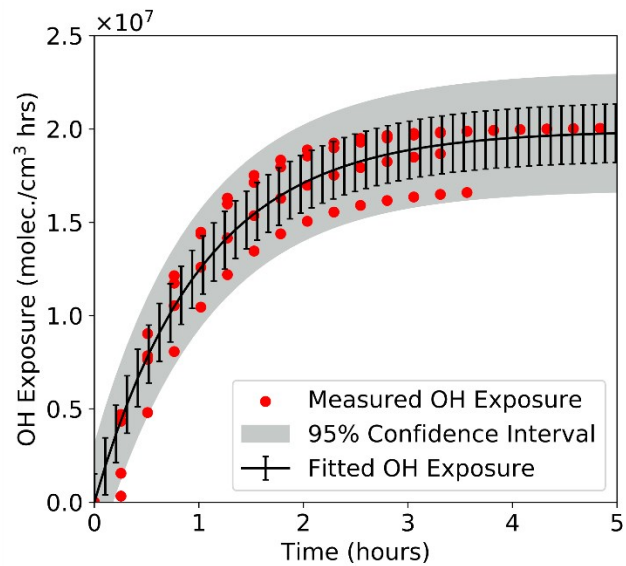


Figure S3: OH exposure calculated based on the decay of toluene in four separate experiments (red circles), along with the fit to the combined data (black lines).

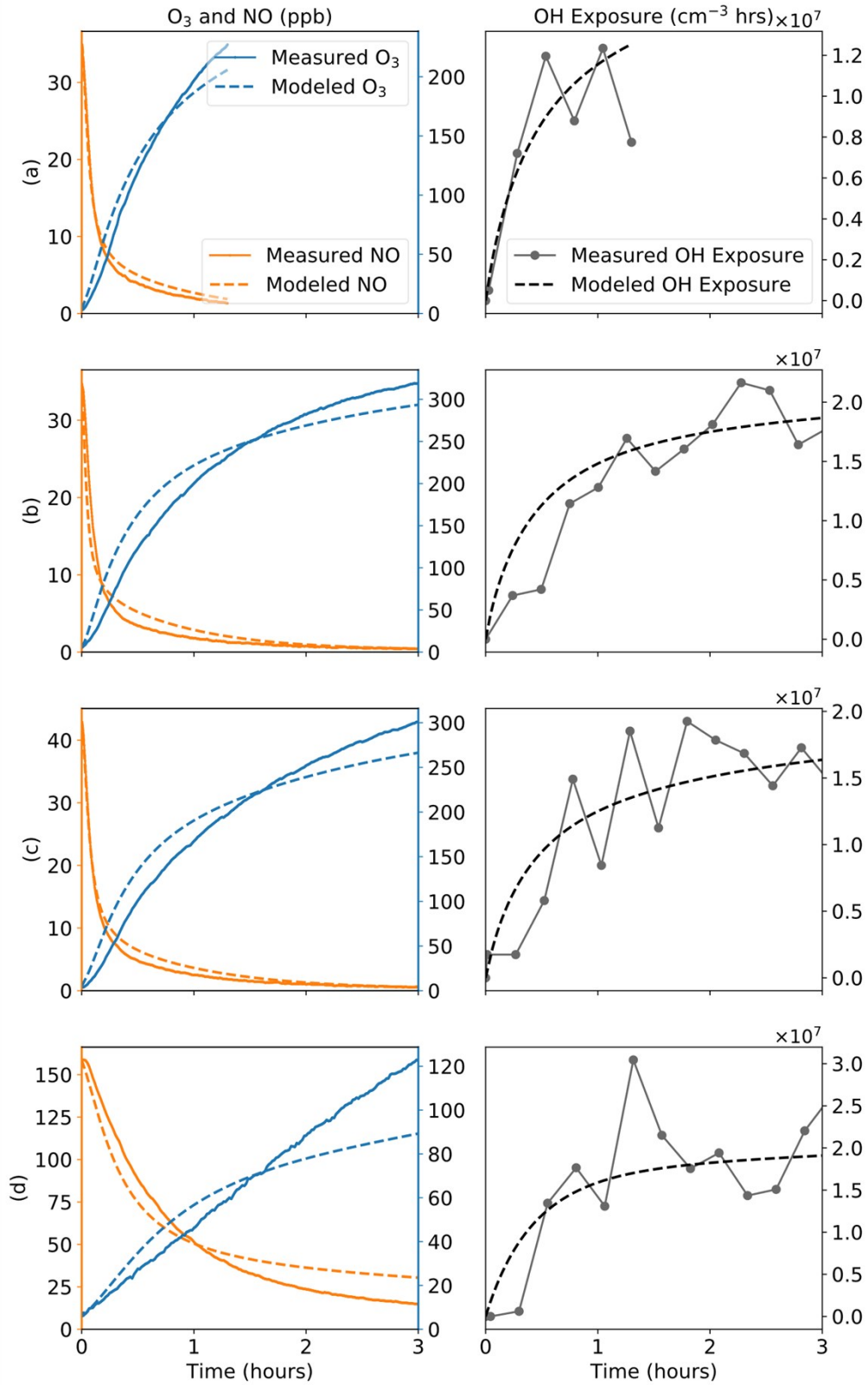


Figure S4: SAPRC model predictions of OH exposure compared to measurements when the model is constrained to O_3 and NO measurements for the four toluene experiments.

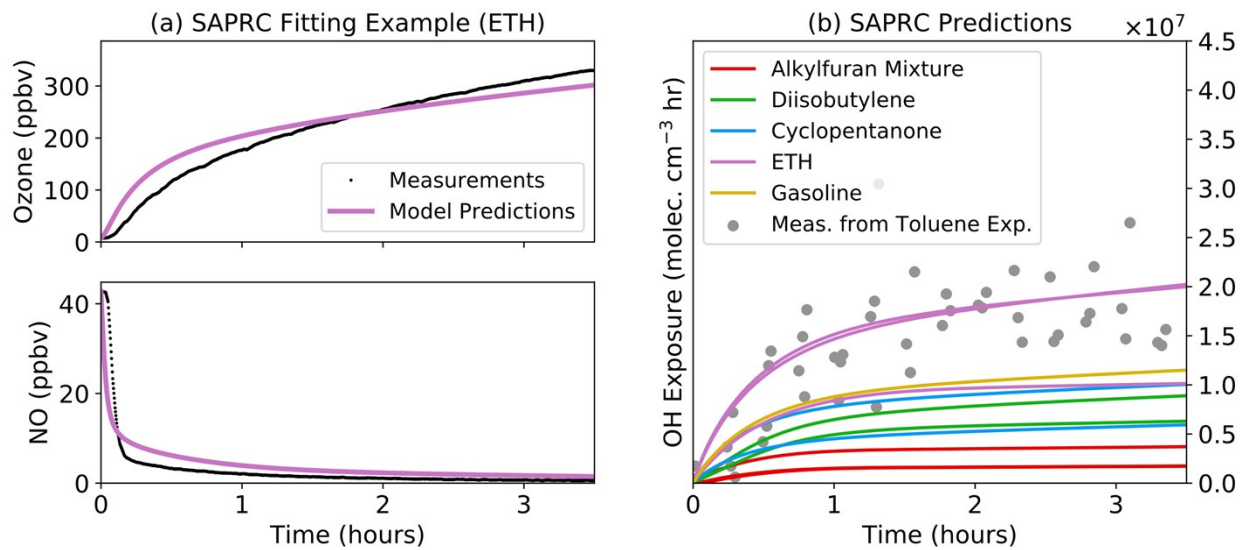


Figure S5: SAPRC model predictions of OH exposures when constrained to O_3 and NO measurements. An example of fitting the model is shown in panel (a). The predicted OH exposures for all fuel experiments are shown in panel (b).

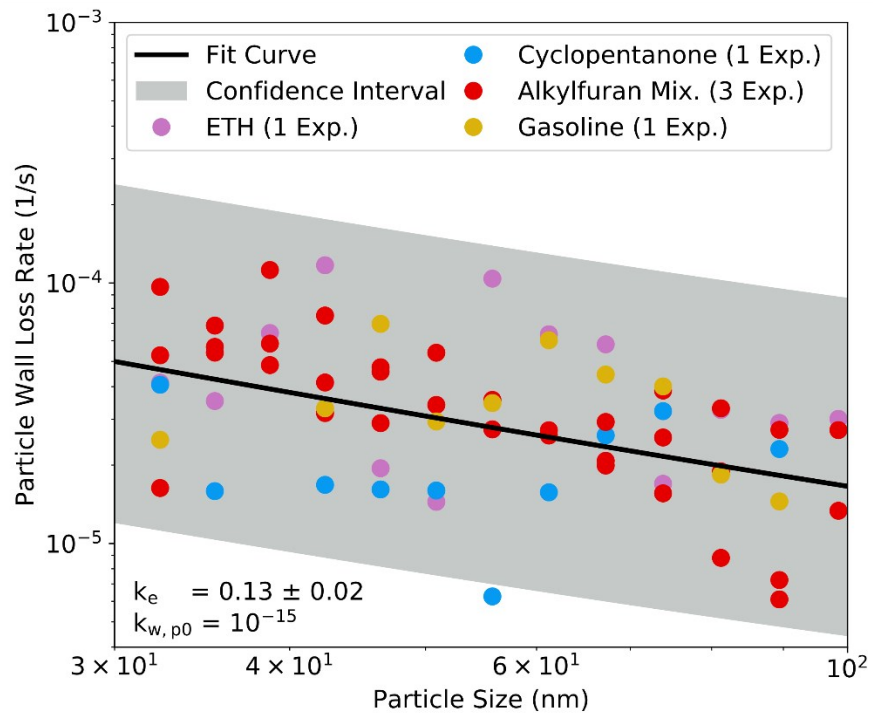


Figure S6: Particle wall loss rates calculated for particle sizes up to 100 nm for six experiments performed in this work. The solid black line represents the best fit to the data while the grey bands represent the 95 percent confidence interval.

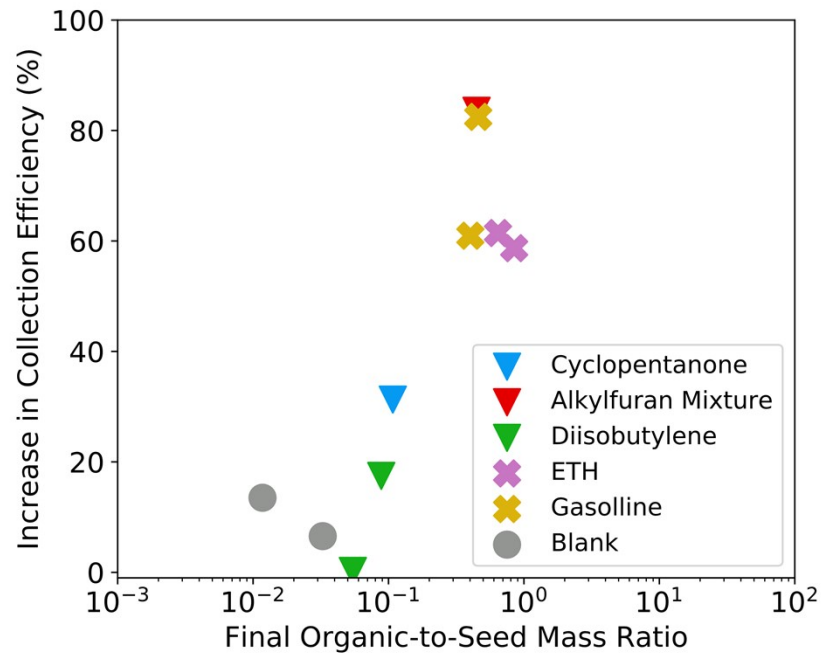


Figure S7: Scaling factor as a function of the organic-to-seed mass ratio for all experiments performed in this work where we had access to the SMPS and ACSM data.

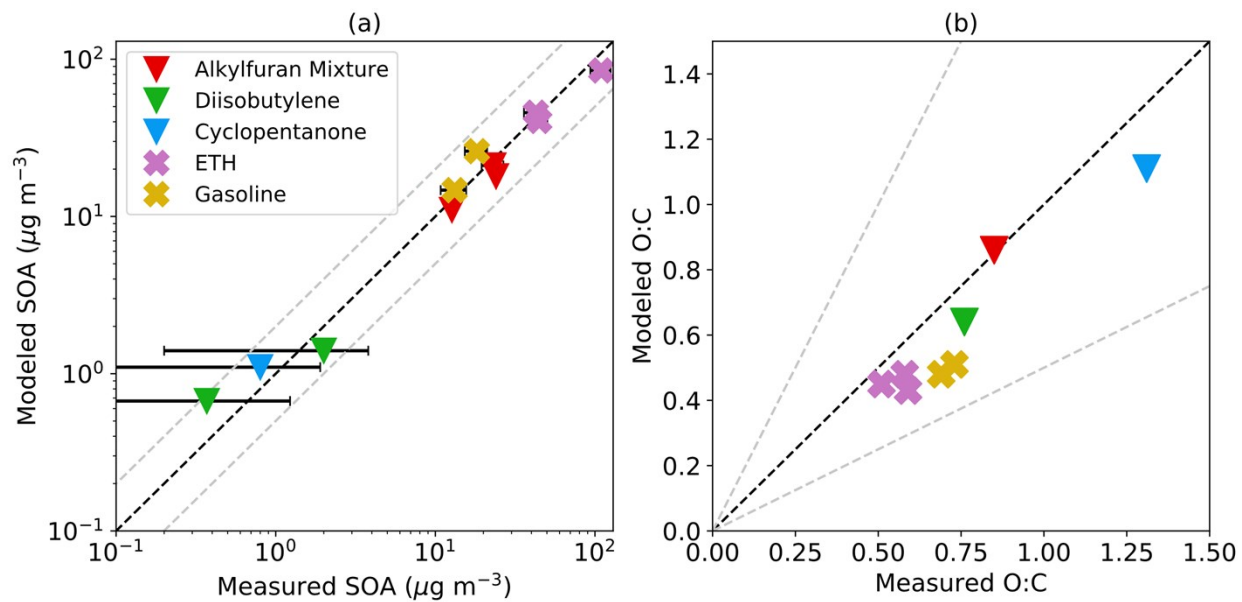


Figure S8: Scatter plot comparing the modeled and measured SOA mass concentrations and O:C for experiments performed in this work.

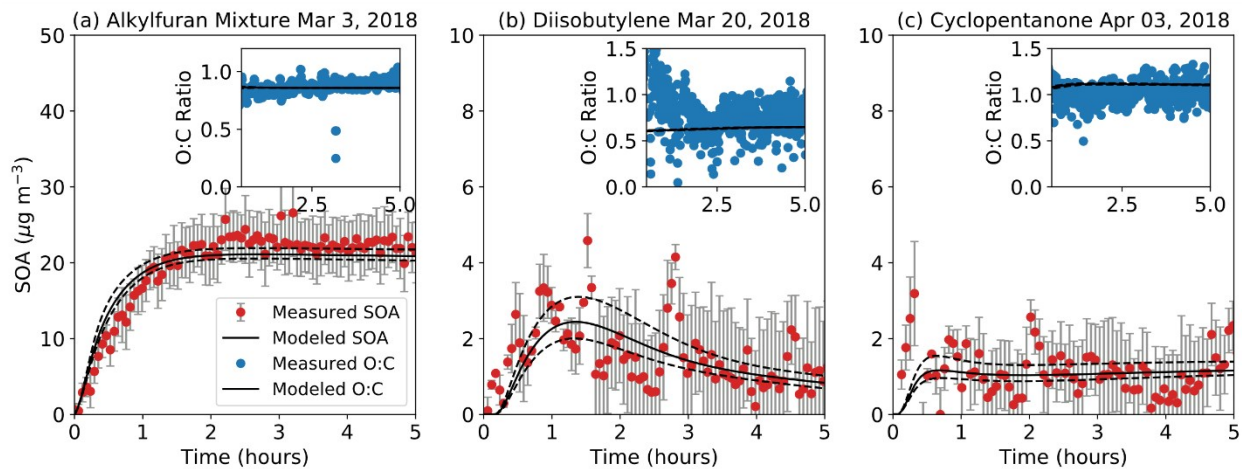


Figure S9: Same as Figure 2 but includes SOM-TOMAS predictions based on a k_e of 0.09 (upper bound) and 0.17 (lower bound) s^{-1} .

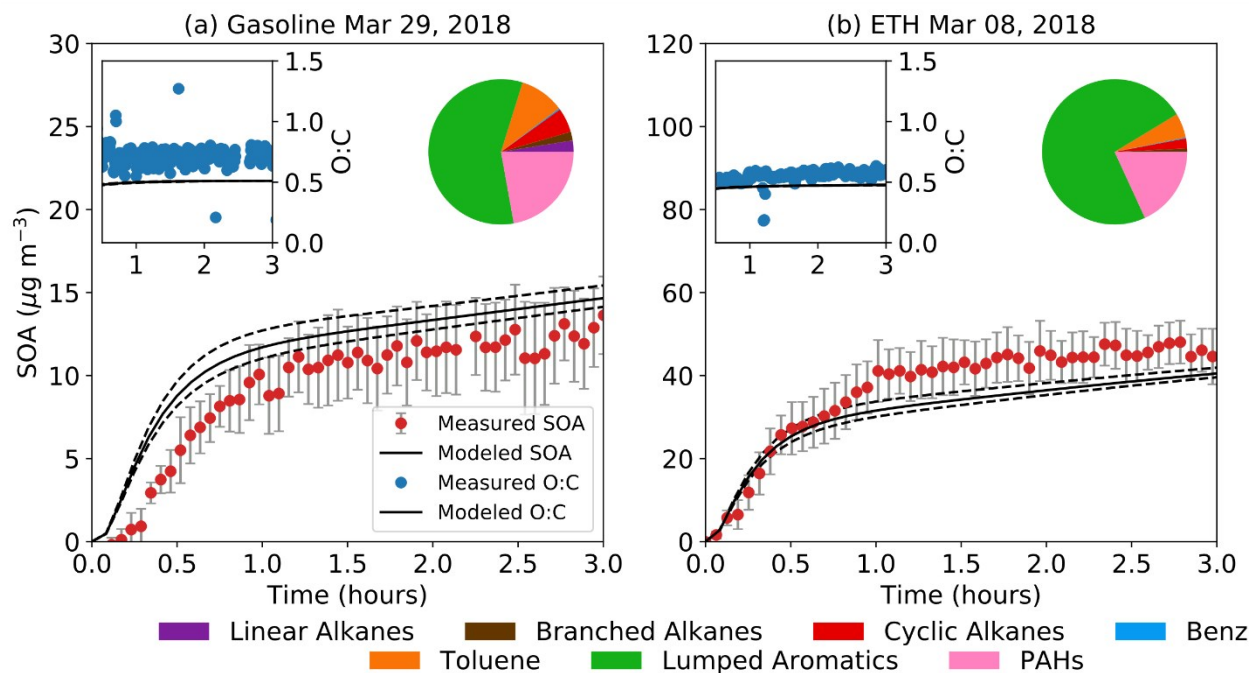


Figure S10: Same as Figure 3 but includes SOM-TOMAS predictions based on k_e of 0.09 (upper bound) and 0.17 (lower bound) s^{-1} .

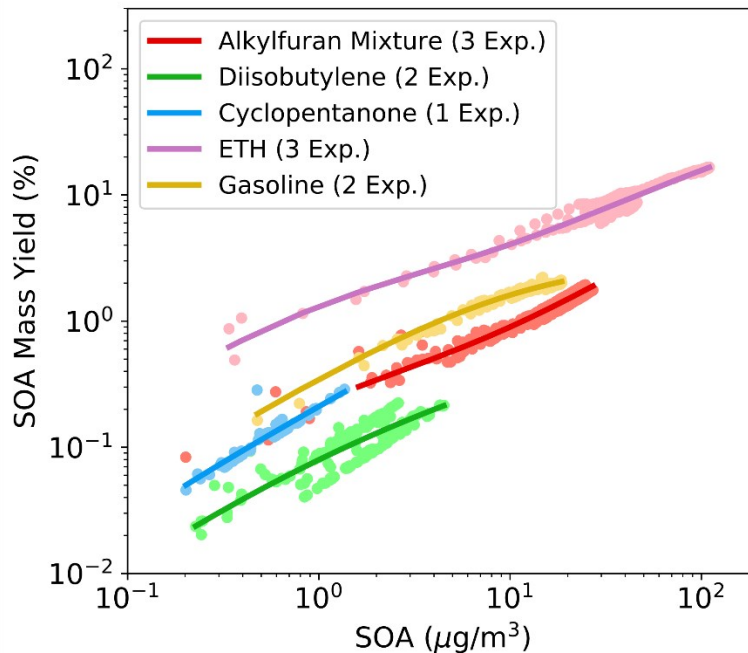


Figure S11: Plot showing the SOA mass yields estimated from the chamber experiments plotted against the SOA mass concentrations for all the experiments performed in this work. The dark solid lines show the fuel-specific volatility basis set (VBS) fits to the data. The VBS fits are shown in Table S.2.

Table S1: SOM grids, surrogate species, and parameters used to model the SOA formation from gasoline and ETH. These parameters have been developed based on data from earlier work.^{6,17}

SOM Grid	Surrogate	m_{frag}	ΔLVP	p_{f1}	p_{f2}	p_{f3}	p_{f4}	Reference
Linear Alkanes	n-dodecane	0.2627	1.4629	0.9657	0.0010	0.0020	0.0314	Loza et al. ¹⁹
Branched Alkanes	methylundecane	0.2042	0.9679	0.3169	0.1804	0.4760	0.0267	Loza et al. ¹⁹
Cyclic Alkanes	hexylcyclohexane	0.2717	1.7950	0.9589	0.0007	0.0014	0.0390	Loza et al. ¹⁹
Benzene	benzene	0.7895	1.5495	0.0743	0.0213	0.8963	0.0081	Ng et al. ⁴
Toluene	toluene	1.3064	1.4169	0.5634	0.3413	0.0016	0.0937	Zhang et al. ⁶
Lumped Aromatics	m-xylene	0.0736	1.4601	0.1418	0.2971	0.4571	0.1040	Ng et al. ⁴
Lumped Aromatics	o-xylene	0.0590	1.3930	0.1260	0.0490	0.7690	0.0570	Song et al. ¹⁸
PAHs	naphthalene	0.7673	1.4922	0.8138	0.0072	0.0635	0.1155	Chan et al. ²⁰

References

- (1) Aljawhary, D.; Lee, A. K. Y.; Abbatt, J. P. D. High-Resolution Chemical Ionization Mass Spectrometry (ToF-CIMS): Application to Study SOA Composition and Processing. *Atmospheric Measurement Techniques* 2013, 6 (11), 3211–3224.
- (2) Lee, B. H.; Lopez-Hilfiker, F. D.; Mohr, C.; Kurtén, T.; Worsnop, D. R.; Thornton, J. A. An Iodide-Adduct High-Resolution Time-of-Flight Chemical-Ionization Mass Spectrometer: Application to Atmospheric Inorganic and Organic Compounds. *Environ. Sci. Technol.* 2014, 48 (11), 6309–6317.
- (3) Lopez-Hilfiker, F. D.; Mohr, C.; D'Ambro, E. L.; Lutz, A.; Riedel, T. P.; Gaston, C. J.; Iyer, S.; Zhang, Z.; Gold, A.; Surratt, J. D.; Others. Molecular Composition and Volatility of Organic Aerosol in the Southeastern US: Implications for IEPOX Derived SOA. *Environ. Sci. Technol.* 2016, 50 (5), 2200–2209.
- (4) Ng, N. L.; Kroll, J. H.; Chan, A. W. H.; Chhabra, P. S.; Flagan, R. C.; Seinfeld, J. H. Secondary Organic Aerosol Formation from *m*-Xylene, Toluene, and Benzene. *Atmos. Chem. Phys.* 2007, 7 (14), 3909–3922.
- (5) Presto, A. A.; Miracolo, M. A.; Donahue, N. M.; Robinson, A. L. Secondary Organic Aerosol Formation from High-NO(x) Photo-Oxidation of Low Volatility Precursors: *n*-Alkanes. *Environ. Sci. Technol.* 2010, 44 (6), 2029–2034.
- (6) Zhang, X.; Cappa, C. D.; Jathar, S. H.; McVay, R. C.; Ensberg, J. J.; Kleeman, M. J.; Seinfeld, J. H. Influence of Vapor Wall Loss in Laboratory Chambers on Yields of Secondary Organic Aerosol. *Proc. Natl. Acad. Sci. U. S. A.* 2014, 111 (16), 5802–5807.
- (7) Isaacman-VanWertz, G.; Massoli, P.; O'Brien, R. E.; Nowak, J. B.; Canagaratna, M. R.; Jayne, J. T.; Worsnop, D. R.; Su, L.; Knopf, D. A.; Misztal, P. K.; Arata, C.; Goldstein, A. H.; Kroll, J. H. Using Advanced Mass Spectrometry Techniques to Fully Characterize Atmospheric Organic Carbon: Current Capabilities and Remaining Gaps. *Faraday Discuss.* 2017, 200, 579–598.
- (8) Saunders, S. M.; Jenkin, M. E.; Derwent, R. G.; Pilling, M. J. Protocol for the Development of the Master Chemical Mechanism, MCM v3 (Part A): Tropospheric Degradation of Non-Aromatic Volatile Organic Compounds. *Atmos. Chem. Phys.* 2003, 3 (1), 161–180.
- (9) Jenkin, M. E.; Saunders, S. M.; Wagner, V.; Pilling, M. J. Protocol for the Development of the Master Chemical Mechanism, MCM v3 (Part B): Tropospheric Degradation of Aromatic Volatile Organic Compounds. *Atmos. Chem. Phys.* 2003, 3 (1), 181–193.
- (10) Aumont, B.; Szopa, S.; Madronich, S. Modelling the Evolution of Organic Carbon during Its Gas-Phase Tropospheric Oxidation: Development of an Explicit Model Based on a Self-Generating Approach. *Atmospheric Chemistry and Physics Discussions.* 2005, pp 703–754.
- (11) Hildebrandt, L.; Donahue, N. M.; Pandis, S. N. High Formation of Secondary Organic Aerosol from the Photo-Oxidation of Toluene. *Atmos. Chem. Phys.* 2009, 9 (9), 2973–2986.
- (12) Pierce, J. R.; Engelhart, G. J.; Hildebrandt, L.; Weitkamp, E. A.; Pathak, R. K.; Donahue, N. M.; Robinson, A. L.; Adams, P. J.; Pandis, S. N. Constraining Particle Evolution from Wall Losses, Coagulation, and Condensation-Evaporation in Smog-Chamber Experiments: Optimal Estimation Based on Size Distribution Measurements. *Aerosol Science and Technology.* 2008, pp 1001–1015.
- (13) McMurry, P. H.; Grosjean, D. Photochemical Formation of Organic Aerosols: Growth Laws and Mechanisms. *Atmospheric Environment (1967).* 1985, pp 1445–1451.
- (14) McMurry, P. H.; Grosjean, D. Gas and Aerosol Wall Losses in Teflon Film Smog

- Chambers. *Environ. Sci. Technol.* 1985, 19 (12), 1176–1182.
- (15) Crump, J. G.; Seinfeld, J. H. Turbulent Deposition and Gravitational Sedimentation of an Aerosol in a Vessel of Arbitrary Shape. *J. Aerosol Sci.* 1981, 12 (5), 405–415.
- (16) Hinds, W. C. *Aerosol Technology: Properties, Behavior, and Measurement of Airborne Particles*; John Wiley & Sons, 1999.
- (17) Cappa, C. D.; Jathar, S. H.; Kleeman, M. J.; Docherty, K. S.; Jimenez, J. L.; Seinfeld, J. H.; Wexler, A. S. Simulating Secondary Organic Aerosol in a Regional Air Quality Model Using the Statistical Oxidation Model - Part 2: Assessing the Influence of Vapor Wall Losses. *Atmos. Chem. Phys.* **2016**, 16 (5), 3041–3059.
- (18) Song, C.; Na, K.; Warren, B.; Malloy, Q.; Cocker, D. R. Secondary Organic Aerosol Formation from the Photooxidation of p - and o -Xylene. *Environ. Sci. Technol.* 2007, 41 (21), 7403–7408.
- (19) Loza, C. L.; Craven, J. S.; Yee, L. D.; Coggon, M. M.; Schwantes, R. H.; Shiraiwa, M.; Zhang, X.; Schilling, K. A.; Ng, N. L.; Canagaratna, M. R.; et al. Secondary Organic Aerosol Yields of 12-Carbon Alkanes. *Atmos. Chem. Phys.* 2014, 14 (3), 1423–1439.
- (20) Chan, A. W. H.; Kautzman, K. E.; Chhabra, P. S.; Surratt, J. D.; Chan, M. N.; Crouse, J. D.; Kürten, A.; Wennberg, P. O.; Flagan, R. C.; Seinfeld, J. H. Secondary Organic Aerosol Formation from Photooxidation of Naphthalene and Alkylnaphthalenes: Implications for Oxidation of Intermediate Volatility Organic Compounds (IVOCs). *Atmos. Chem. Phys.* 2009, 9 (9), 3049–3060.